Acta Oceanol. Sin., 2024, Vol. 43, No. 1, P. 123–134
https://doi.org/10.1007/s13131-024-2345-4
http://www.aosocean.com
E-mail: ocean2@hyxb.org.cn

A positive trend in the stability of global offshore wind energy

Chongwei Zheng[1, 2, 3*]

[1] Dalian Naval Academy, Dalian 116018, China

[2] Marine Resources and Environment Research Group on the Maritime Silk Road, Dalian 116018, China

[3] Shandong Provincial Key Laboratory of Ocean Engineering, Ocean University of China, Qingdao 266100, China

Received 31 December 2022; accepted 16 March 2023

Abstract

The recognition on the trend of wind energy stability is still extremely rare, although it is closely related to acquisition efficiency, grid connection, equipment lifetime, and costs of wind energy utilization. Using the 40-year (1979–2018) ERA-Interim data from the European Center for Medium-Range Weather Forecasts, this study presented the spatial-temporal distribution and climatic trend of the stability of global offshore wind energy as well as the abrupt phenomenon of wind energy stability in key regions over the past 40 years with the climatic analysis method and Mann-Kendall (M-K) test. The results show the following 5 points. (1) According to the coefficient of variation (C_v) of the wind power density, there are six permanent stable zones of global offshore wind energy: the southeast and northeast trade wind zones in the Indian, Pacific and Atlantic oceans, the Southern Hemisphere westerly, and a semi-permanent stable zone (North Indian Ocean). (2) There are six low-value zones for both seasonal variability index (S_v) and monthly variability index (M_v) globally, with a similar spatial distribution as that of the six permanent stable zones. M_v and S_v in the Arabian Sea are the highest in the world. (3) After C_v, M_v and S_v are comprehensively considered, the six permanent stable zones have an obvious advantage in the stability of wind energy over other sea areas, with C_v below 0.8, M_v within 1.0, and S_v within 0.7 all the year round. (4) The global stability of offshore wind energy shows a positive climatic trend for the past four decades. C_v, M_v and S_v have not changed significantly or decreased in most of the global ocean during 1979 to 2018. That is, wind energy is flat or more stable, while the monthly and seasonal variabilities tend to shrink/smooth, which is beneficial for wind energy utilization. (5) C_v in the low-latitude Pacific and M_v and S_v in both the North Indian Ocean and the low-latitude Pacific have an obvious abrupt phenomenon at the end of the 20th century.

Key words: global oceans, wind energy, stability, spatial-temporal distribution, climatic trend

Citation: Zheng Chongwei. 2024. A positive trend in the stability of global offshore wind energy. Acta Oceanologica Sinica, 43(1): 123–134, doi: 10.1007/s13131-024-2345-4

1 Introduction

With the rapid development of human society, how to deal with the severe energy crisis and environment crisis is a common difficulty faced by all countries. However, the World Meteorological Organization (WMO) released the latest edition of the latest WMO Greenhouse Gas Bulletin and pointed out that the increase in CO_2 concentrations in 2020–2021 is greater than the average annual growth rate over the past decade. How can we break the energy crisis while ensuring sustainable development? Offshore wind energy is known as renewable energy that has the characteristics of nonpolluting, large storage, and wide distribution. It has been paid more attention by more and more countries. The reasonable utilization of wind energy resources will ease the energy crisis, protect the ocean environment, promote deep-sea development, and promote tourism in remote islands (Xydis, 2015; Soukissian and Karathanasi, 2016; Soukissian et al., 2017). Due to different spatial-temporal distributions of wind energy resources, the basic principle of wind energy utilization is the priority evaluation of resource (Xydis and Mihet-Popa, 2017; Langodan et al., 2014, 2016). On the basis of a detailed investigation of resource features, an orderly plan for energy development and power grid construction can be formulated (Wan et al., 2018).

Previous researchers have contributed many excellent studies on the wind energy evaluation, such as the spatial-temporal distribution (Chadee and Clarke, 2014; Carvalho et al., 2014; Esteban et al., 2019; Ulazia et al., 2017; Zheng et al., 2019a), energy classification (Zheng et al., 2018, 2019b), short-term forecasting of energy (Liu and Chen, 2019; Han et al., 2015; Allen et al., 2017; Qian et al., 2019), and long-term projections of energy (Davy et al., 2018; Carvalho et al., 2017b). According to the data sources, wind energy evaluations have gone through three typical stages: observation data stage, simulation data stage and reanalysis data stage. González-Longatt et al. (2014) found that the best wind energy was located in the northern coastal area of Venezuela based on observation data from 32 meteorological stations, which provided a scientific and detailed reference for wind energy development in this region. Liu et al. (2019) presented the wind potential of China using observations from 2 430 meteorological stations for the period of 2006–2015. The Northeast China

Foundation item: The Open Fund Project of Shandong Provincial Key Laboratory of Ocean Engineering, Ocean University of China under contract No. kloe201901; the Open Research Fund of State Key Laboratory of Estuarine and Coastal Research under contract No. SKLEC-KF201707.

*Corresponding author, E-mail: chinaoceanzcw@sina.cn

was found to have the highest wind energy of 204 W/m^2. The global usable wind energy in the ocean was evaluated by Capps and Zender (2010) for the first time. They found that the mean wind power density (WPD) increased by 30%, 69%, and 73% from 10 m to 100 m in the tropics, Southern Hemisphere extra-tropics, and Northern Hemisphere extra-tropics, respectively. Onea et al. (2016) analyzed the wind energy along the Mediterranean Sea coasts. More energetic wind conditions were found in the northern part of the basin and southern part of the sea. Wang et al. (2019) provided a wind energy evaluation of the coast of central California and found that the WIND Toolkit has the best data for this area. Rusu et al. (2018) presented a joint analysis of wind and wave energy in the Black Sea. The suitable regions for combined wave-wind utilization in this region were exhibited for the first time. Yan et al. (2019) filled the research gap on model evaluation. Omrani et al. (2017) analyzed the response of wind energy to sea surface temperature in the northwestern Mediterranean Sea based on three 20-year simulations. The WPD varied by 6%–12% for the control simulation data versus the smoothed simulation data, and by –5% to –7.5% for the coupled simulation data versus the smoothed simulation data. Allouhi et al. (2017) evaluated the wind energy potential of the Moroccan coast using the least squares, maximum likelihood, and WAsP methods. Dakhla and Laayoune were found to be the suitable sites of energy development. Carvalho et al. (2017a) evaluated wind energy by using Advanced Scatterometer (ASCAT), Ocean SCATterometer (OSCAT), Weather Research and Forecast (WRF) models and buoys data. This study has an important reference value for energy utilization in regions without observation data. Thomas et al. (2008) found a global oceanic increasing trend of wind speed (2–4 cm/(s·a)) for 1982–2002 based on the International Comprehensive Ocean–Atmosphere Data Set (ICOADS). Zheng et al. (2017) found an increasing trend of WPD of 4.45 W/(m^2·a) in the North Atlantic Ocean for 1988–2011 with cross-calibrated, multiplatform (CCMP) data. And a close relationship between wind energy and the North Atlantic Oscillation (NAO) and El Niño phenomenon in this region was found. Costoya et al. (2021) carried out an in-depth study of the climate change impact on the offshore wind energy resource in China. And a novel classification for the future wind energy was presented, which provided an important reference for the long-term wind energy development. Jung et al. (2019) exhibited the long-term trends and interannual variability of global wind energy. No significant variations were found in China and Germany.

Predecessors have contributed a lot to the analysis of spatial-temporal characteristics of wind energy. However, the studies on the climatic variation in wind energy are still rare, although they are related to long-term development plans. Overall, the few existing studies on wind energy trends are mainly about the trend of wind speed or the trend of WPD. Research on the climatic trend of wind energy stability is still in the blank, although it is closely related to the capture efficiency and conversion efficiency. In actual wind energy development, resource stability is closely related to acquisition efficiency, grid connection, lifetime of equipment, and costs (Pryor and Barthelmie, 2011; Rusu and Onea, 2017). The climatic variation in wind energy stability has an important influence on the location of wind power plant and development planning in medium and long terms. As a result, this study pays attention to the long-term variation in wind energy stability in global oceans for the first time by using ERA-Interim data from the European Center for Medium-Range Weather Forecasts (ECMWF), to provide a scientific reference for the planning of resource development.

2 Data and methodology

2.1 *Data*

Commonly used reanalysis wind production includes the CCMP, 45-year ECMWF (ERA-40), ERA-Interim and so on. The time series of CCMP is from July 1987 to April 2019. The time series of ERA-40 is from September 1957 to August 2002. The time series of ERA-Interim is from January 1979 to August 2019. This study aims to reveal the climatic variation in the stability of global oceanic wind energy for the last 40 years. As a result, ERA-Interim is employed in this study. The ERA-Interim data are provided by the ECMWF (Dee et al., 2011), with spatial range covering the world (180°W–180°E, 90°S–90°N) and a time series from January 1979 to August 2019. The time series of 1979–2018 is selected here to exhibit the climatic variation of the global oceanic wind energy stability over the past 40 years. The spatial resolutions include 0.125° × 0.125°, 0.25° × 0.25°, 0.5° × 0.5°, 0.75° × 0.75°, ⋯, 1.25° × 1.25°, and 2.5° × 2.5°. Song et al. (2015), Kumar et al. (2013) and Wang et al. (2020) compared the ERA-Interim data with observations data. And a good agreement was found. The ERA-Interim reanalysis data have also been widely used in the analysis of wind variability in Antarctica (Yu and Zhong, 2019), global near-surface wind speed (Marcos et al., 2019), and energy evaluation (Zheng et al., 2019b; Wan et al., 2015).

2.2 *Calculation method of wind energy stability*

Cornett (2008) demonstrated the stability of wave energy resources by calculating the coefficient of variation (C_v), seasonal variability index (S_v) and monthly variability index (M_v) of wave power density. However, so far, the research on wind energy stability has been rare. With the reference to the method provided by Cornett, the three important parameters (C_v, M_v and S_v) are used to exhibit the characteristics of global oceanic wind energy stability. With the 6-hourly ERA-Interim data for January 1, 1979 to December 31, 2018 and calculation method of WPD, the 6-hourly WPD for the past 40 years is obtained. Then with the reference to Cornett (2008), C_v, S_v and M_v of WPD are calculated to exhibit the characteristics of wind energy stability. The analysis of wind energy stability in this study mainly includes the following work. Firstly, the spatial and temporal distribution characteristics of C_v, S_v and M_v of global oceanic WPD are analyzed by using climate analysis methods. Secondly, the climatic trend of C_v, S_v and M_v of global oceanic WPD for the past 40 years is analyzed by using moving average method and linear regression, as well as the trends of wind energy stability in key regions, systematically including the overall trend, the regional and seasonal differences of the climatic trend. Thirdly, the Mann-Kendall (M-K) test is employed to calculate the abrupt phenomenon of C_v, S_v and M_v of WPD in key regions. A schematic diagram of this study is shown in Fig. 1.

The calculation method of WPD is described as follows (Capps and Zender, 2010; Liu et al., 2019):

$$\mathrm{WPD} = \frac{1}{2}\rho U^3, \tag{1}$$

where WPD is the wind power density (unit: W/m^2), U is the wind speed (unit: m/s), and ρ is the sea level air density (1.225 kg/m^3) (Capps and Zender, 2010).

According to the calculation method of C_v of wave energy presented by Cornett (2008), C_v is calculated as

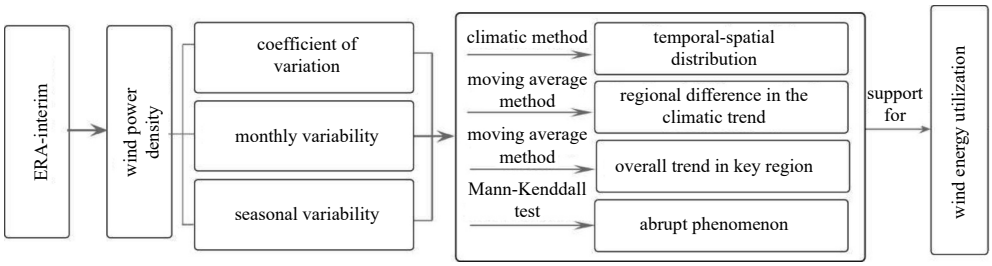

Fig. 1. Schematic diagram of the climatic trend analysis of the stability of global oceanic wind energy.

$$C_{\mathrm{v}} = \frac{S}{\bar{x}}, \tag{2}$$

where C_{v} is the coefficient of variation. The smaller C_{v} is, the better the energy stability is. $\bar{x}$ is the average value of the WPD. S is the standard deviation and is calculated as

$$S = \sqrt{\frac{\sum_{i=1}^{n} x_i^2 - \left(\sum_{i=1}^{n} x_i\right)^2 / n}{n-1}}, \tag{3}$$

where n is the number of data points.

According to the calculation method of M_{v} of wave energy presented by Cornett (2008), M_{v} is calculated as

$$M_{\mathrm{v}} = \frac{P_{m1} - P_{m2}}{P_{\mathrm{year}}}, \tag{4}$$

where P_{m1} is the month with the largest WPD value, P_{m2} is the month with the smallest WPD value, and P_{year} is the annual mean WPD value. The greater the M_{v} is, the worse the monthly stability is.

According to the calculation method of S_{v} of wave energy presented by Cornett (2008), S_{v} is calculated as

$$S_{\mathrm{v}} = \frac{P_{s1} - P_{s4}}{P_{\mathrm{year}}}, \tag{5}$$

where P_{s1} is the season with the highest WPD value, P_{s4} is the season with the smallest WPD value, and P_{year} is the annual mean WPD value. The greater the S_{v} is, the poorer the seasonal stability is.

3 Spatial-temporal distribution of wind energy stability

3.1 *Coefficient of variation*

3.1.1 *Multi-year average status for the past 40 years*

With the 6-hourly WPD value from 00:00 March 1, 1979 to 18:00 May 31, 1979, the average value of C_{v} in March-April-May (MAM) 1979 was obtained. Similarly, the C_{v} in every MAM for 40 years was calculated. Then, the multi-year average C_{v} in MAM for the past 40 years at each grid point was calculated, as shown in Fig. 2a. With the same method, the multi-year average values of C_{v} in June-July-August (JJA), September-October-November (SON), and December-January-February (DJF) for the past 40 years were also obtained (Fig. 2). A smaller C_{v} indicates better energy stability, which is beneficial for power utilization.

Overall, the C_{v} in the offshore is smaller than that in the nearshore in each season, meaning a better energy stability in the offshore. C_{v} in the trade wind areas and monsoon areas is smaller than that in other sea areas, meaning that the stability in the trade wind areas and monsoon areas is better than that in other sea areas. The stability in the Southern Hemisphere westerly is better than that in the Northern Hemisphere. The stability in the North Pole is more stable than that in the South Pole. Greenland and the South Pole have the worst wind energy stability in the

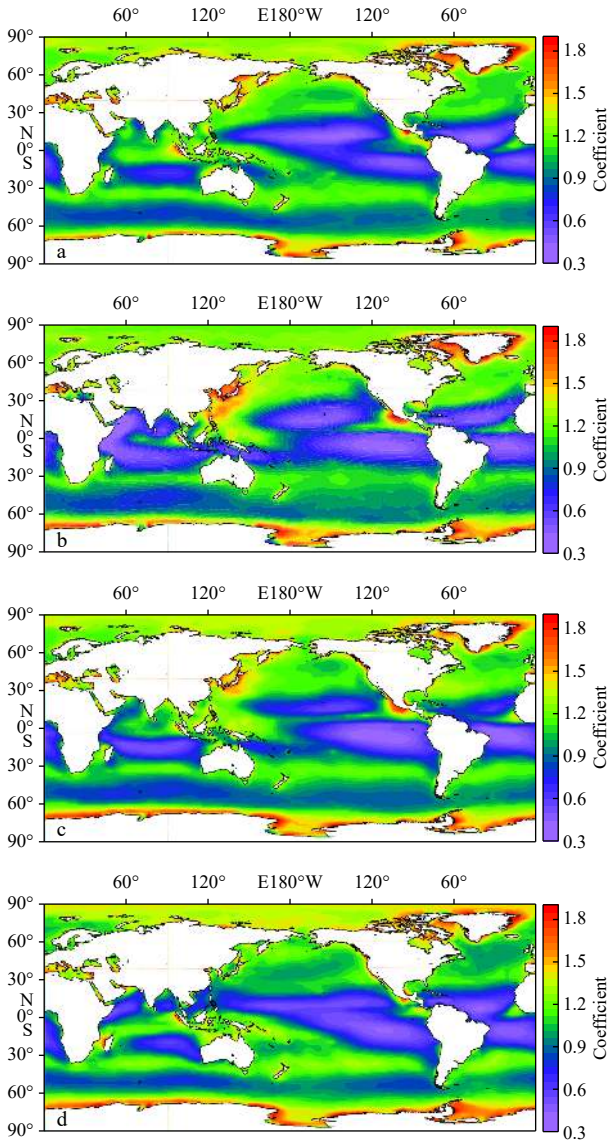

Fig. 2. Multi-year average coefficient of variation of wind power density in MAM (a), JJA (b), SON (c), and DJF (d) for the period 1979–2018.

world. The stability in the equatorial Indian Ocean, Indonesian waters, and western Mexico is relatively poorer than that in other low-latitude areas. At middle latitudes, the relatively poor-stability areas are distributed near the shore of the Northwest Pacific Ocean, the Mozambique Channel, and 30°S waters.

There are 6 zones with good perennial stability in the world: the northeast trade wind area in the North Pacific, the southeast trade wind area in the South Pacific, the northeast trade wind area in the Atlantic, the southeast trade wind area in the South Atlantic, the southeast trade wind area in South Indian Ocean, and the Southern Hemisphere westerly waters, with C_v values lower than 0.8 all the year round. Here, the area with C_v below 0.8 all the year round is defined as the permanent stable zone. In addition, the monsoon area in the North Indian Ocean has a good stability in summer and winter monsoon wind periods and has a poor stability in the monsoon transition season. Here, area with C_v below 0.8 in partial months but not all the year round is defined as the semi-permanent stable zone.

It is worth noting that there are several obviously large value areas of C_v, meaning a poor wind energy stability in these regions. In the waters around the Greenland, C_v is greater than 1.5 all the year round, even up to 1.8 in the large center. In the coast of the South Pole, C_v is high all the year round. The area range with C_v above 1.5 is largest in JJA and DJF, followed by SON, and smallest in MAM. In the waters around Japan Sea and Ryukyu Islands, C_v is largest in JJA, followed by MAM and SON, and smallest in DJF.

The best season for the stability of wind energy varies from sea to sea. The wind energy stability in the Northwest Pacific Ocean is best in DJF and worst in JJA. The North Indian Ocean is best in JJA, followed by DJF, and worst in MAM. The southeast trade wind area in the South Indian Ocean is best in JJA, followed by SON, and worst in DJF. The southeast trade wind areas of the Pacific and Atlantic are best in SON, followed by JJA, and worst in MAM. The northeast trade wind areas of the Pacific and Atlantic are best in MAM and worst in SON. The stability of the westerly zone in the Southern and Northern Hemispheres is best in their respective winters and worst in summer.

3.1.2 *Multi-year average status for different decades*

By averaging the C_v in every JJA for the period of 1979–1988 obtained in Section 3.1.1, the multi-year average C_v in JJA for the first decade (1979–1988) was calculated, as shown in Fig. 3a. Similarly, the multi-year average C_v in JJA for the decades of 1979–1988, 1989–1998, 1999–2008, and 2009–2018 was obtained respectively, as shown in the left side of Fig. 3. With the same method, the multi-year average C_v in DJF for the decades of 1979–1988, 1989–1998, 1999–2008, and 2009–2018 was obtained respectively, as shown in the right side of Fig. 3. The C_v showed a good consistency throughout the decades overall.

In JJA, there is a good agreement between the spatial distribution of C_v for each decade and that of the multi-year average of the past 40 years overall. Areas with significant differences in C_v in different decades are mainly distributed along the coast of the Northwest Pacific Ocean and the South Indian Ocean westerly waters. In the Northwest Pacific Ocean, for the periods of 1979–1988 and 1989–1998, the large-value areas with C_v above 1.5 are mainly distributed in the Bohai Sea, the Yellow Sea and the Japan Sea. For the periods of 1999–2008 and 2009–2018, the area range with C_v above 1.5 in the Northwest Pacific Ocean increased significantly, including the Bohai Sea, the Yellow Sea, the Japan Sea and a large area surrounding the Ryukyu Islands. In the South Indian Ocean westerly for the period of 1979–1988, the area range with C_v below 0.8 was small and mainly distributed near Kerguelen Island. For the periods of 1989–1998, 1999–2008 and 2009–2018, the area range with C_v below 0.8 increased significantly, covering the South Indian Ocean westerly with an east-west banded distribution.

In DJF, there is a good agreement of the spatial distribution of C_v for each decade. Areas with significant differences in C_v in different decades are mainly distributed in the Weddell Sea and in mid-latitudes of the North Atlantic Ocean. In the Weddell Sea, the area range with C_v about 1.6 is smallest for 1989–1998. For 1979–1988, 1999–2008 and 2009–2018, C_v in the entire Weddell Sea was approximately 1.6. At the mid-latitudes of the North Atlantic Ocean, the area range with C_v of approximately 1.0 was largest for 1989–1998.

No matter in JJA or DJF, waters around the Greenland and coast of the South Pole are always the high value areas of C_v, which are the same in all decades. Similarly, no matter in JJA or DJF, the northeast trade wind area in the North Pacific, the southeast trade wind area in the South Pacific, the northeast trade wind area in the Atlantic, the southeast trade wind area in the South Atlantic, the southeast trade wind area in South Indian Ocean, and the Southern Hemisphere westerly waters are always the low value center of C_v, which are the same in all decades.

3.2 *Monthly variability index*

By averaging the 6-hourly WPD from 00:00 January 1, 1979 to 18:00 January 31, 1979, the monthly mean value of WPD in January 1979 was obtained. Similarly, the monthly mean value of WPD in each grid point for each month of 1979 was calculated. Then, M_v of wind power density in 1979 was calculated by using the calculation method of M_v. With the above methods, the year-by-year M_v for 40 years was calculated. Then, M_v for the multi-year average was obtained, as shown in Fig. 4. A smaller M_v indicates a small monthly variation, which is beneficial for power utilization.

Overall, M_v in the Southern Hemisphere is significantly smaller than that in the Northern Hemisphere, meaning that the monthly variation of wind power density in the Southern Hemisphere is smaller than that in the Northern Hemisphere. Six zones with small monthly variations in wind energy in the world are found. Five relatively low-value areas of M_v are located in low-latitude waters (i.e., areas with small monthly variations in wind energy): the southeast trade wind zones in the South Indian Ocean, the South Pacific, the South Atlantic, and the northeast trade wind areas of the Pacific and South Atlantic (with M_v below 1.0). In addition, M_v of the Southern Hemisphere westerly is generally within 1.0. There are five large-value areas of M_v: the North Indian Ocean, tropical South Indian Ocean, western low-latitude Pacific, Northern Hemisphere westerly, and the offshore area of eastern Greenland, with M_v basically above 2.0. It is worth noting that M_v in the Arabian Sea is obviously higher than that in other regions of the global oceans, reaching 3.4. The reason is that the southwest monsoon in this region is very strong in summer, with the average wind force reaching class 6, while the wind force in the monsoon transition period is weak, resulting in a large monthly variation in the WPD. In the Northern Hemisphere westerly, the winter wind is strong, while the summer wind is weak, which causes large differences of wind speeds between winter and summer, resulting in a larger M_v in this region.

By averaging the yearly M_v for the period of 1979–1988, the multi-year average M_v in this decade is calculated. Similarly, the multi-year average M_v for the decades of 1979–1988, 1989–1998,

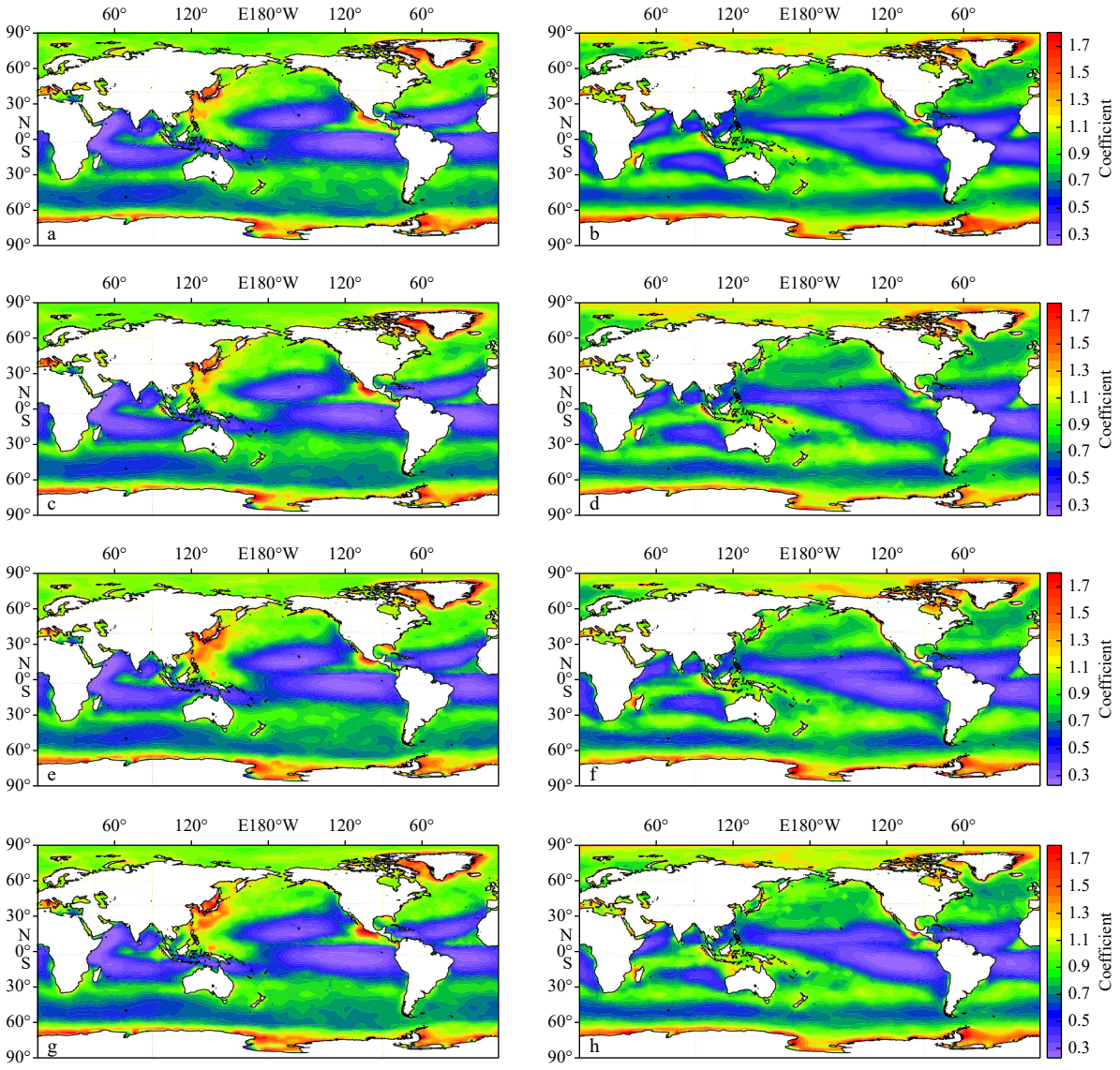

Fig. 3. Coefficient of variation of wind power density for the periods of 1979–1988 (a, b), 1989–1998 (c, d), 1999–2008 (e, f), and 2009–2018 (g, h) in JJA (left) and DJF (right).

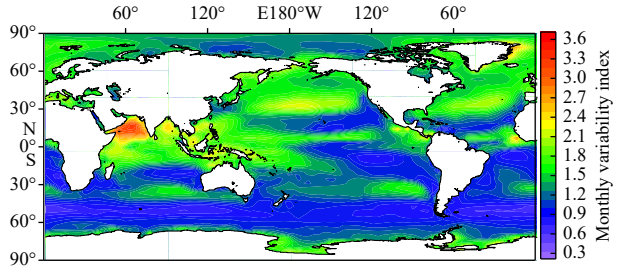

Fig. 4. Monthly variability index of wind power density for the period 1979–2018 in global oceans.

1999–2008, and 2009–2018 is obtained respectively, as shown in Fig. 5. M_v shows a good consistency throughout the decades overall. A good agreement was found in the spatial distribution of M_v for each decade. It is very obvious that the Arabian Sea has the highest M_v in the world, with the value above 3.0. M_v in the Southern Hemisphere westerlies is the lowest, which is within 0.9. M_v in the Southern Hemisphere is significantly smaller than that in the Northern Hemisphere, which is also the same throughout the decades.

Areas with significant differences in M_v in different decades are mainly distributed in the 40°S waters of the South Indian Ocean, as well as in the northeast and southeast trade wind regions of each ocean, especially the 40°S waters of the South Indian Ocean and the northeast trade winds and southeast trade winds areas of the Pacific Ocean. In the 40°S waters of the South Indian Ocean, the area range with M_v about 1.8 is largest in 1999–2008, followed by 1979–1988 and 1989–1998, and smallest in 2009–2018. In the Pacific Ocean, the northeast trade wind area and the southeast trade wind area are the low-value centers of M_v. In the northeast trade winds area, the area range with M_v below 0.9 is largest in 1999–2008, followed by 2009–2018, and smallest in 1989–1998. In the southeast trade winds area, the area range with M_v below 0.9 is largest in 1999–2008 and 2009–2018 and smallest in 1989–1998.

3.3 *Seasonal variability index*

By averaging the WPD from 00:00 March 1, 1979 to 18:00 May

31, 1979, the WPD in MAM 1979 was obtained. Similarly, the WPD was calculated in four seasons of 1979. Then, S_v of wind power density in 1979 was calculated according to the calculation method of S_v. With this method, yearly S_v for the past 40 years was calculated respectively. Then, the multi-year average S_v for the past 40 years was obtained (Fig. 6). Overall, the spatial distribution characteristic of S_v maintains a good consistency with that of M_v, but the value of S_v is slightly lower than that of M_v. The S_v in the Arabian Sea is the largest in the world (mostly above 1.6, with a center above 2.5), followed by the westerly zone of the Northern Hemisphere, the Bay of Bengal, and a narrow east-west belt in the tropical North Pacific.

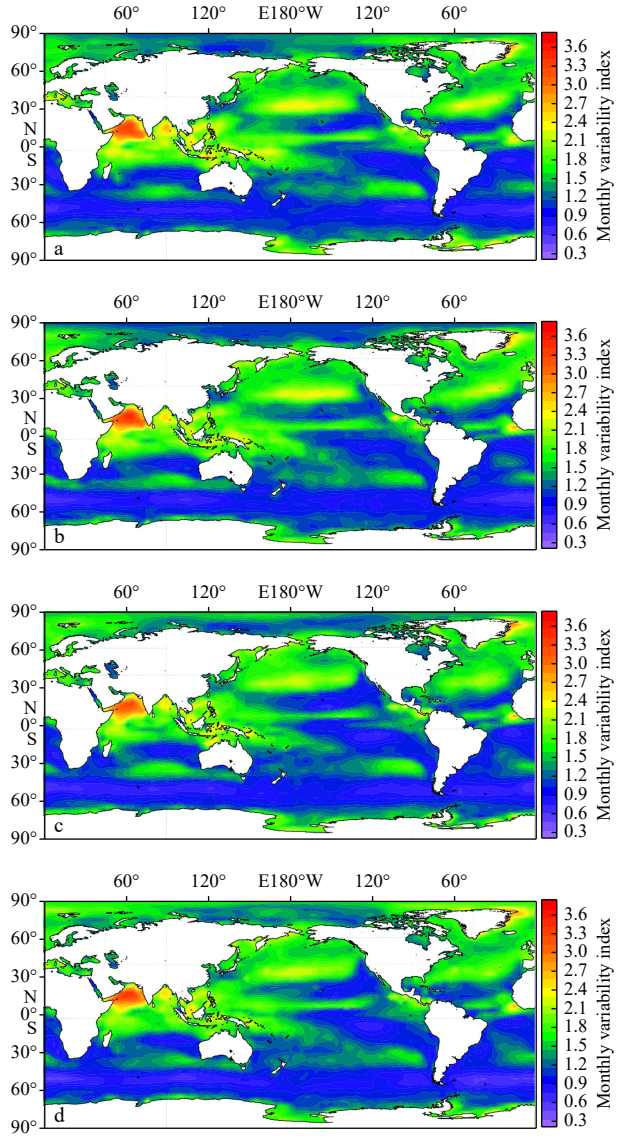

Fig. 5. Monthly variability index of wind power density for the decades 1979–1988 (a), 1989–1998 (b), 1999–2008 (c), and 2009–2018 (d).

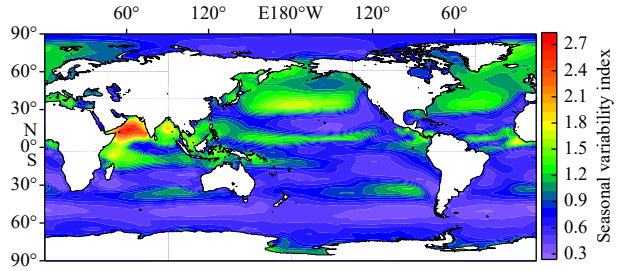

Fig. 6. Seasonal variability index of wind power density in the global oceans for the period 1979–2018.

According to the method in Section 3.2, S_v of each decade was calculated, as shown in Fig. 7. S_v of all decades shows a good consistency, and only in some small sea areas has slight differences. The high-value region is always distributed in the Arabian Sea in all decades, followed by the westerly of the North Pacific Ocean and the westerly of the North Atlantic Ocean.

4 Climatic trend of wind energy stability

4.1 *Coefficient of variation*

Based on the C_v data of each MAM for the past 40 years obtained in Section 3.1.1, moving average method and linear regression were used to calculate the climatic trend of C_v at each

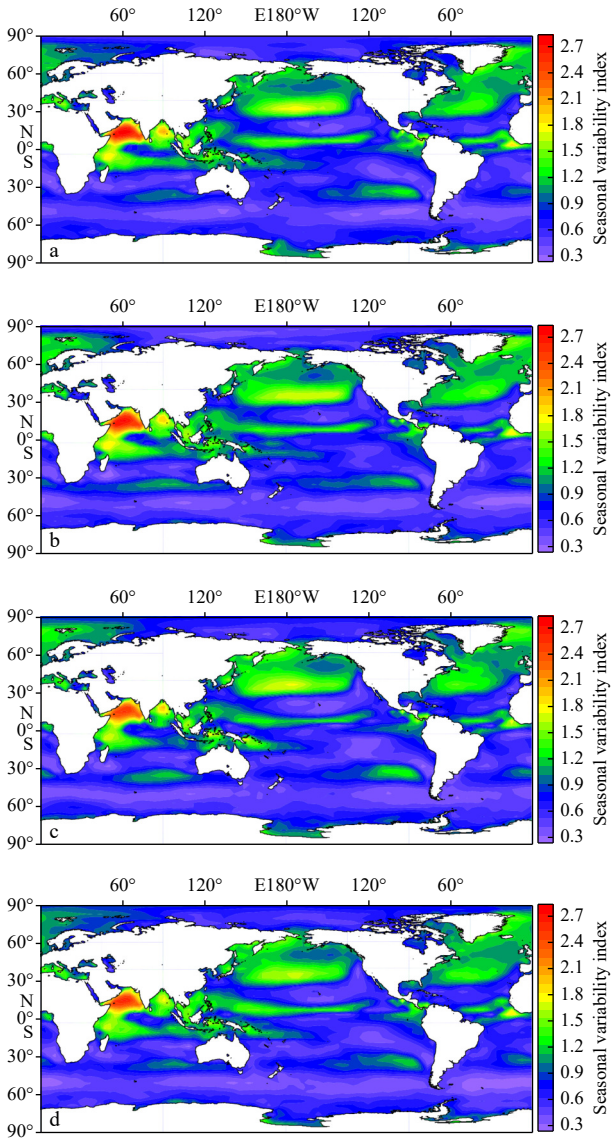

Fig. 7. Seasonal variability index of wind power density for the decades 1979–1988 (a), 1989–1998 (b), 1999–2008 (c), and 2009–2018 (d).

grid point in MAM, as shown in Fig. 8a. Similarly, C_v trends in JJA, SON, and DJF were calculated respectively, as shown in Fig. 8. A decrease in C_v indicates that the wind energy stability tends to be better, while an increase in C_v indicates a worse trend in wind energy stability. No significant change in C_v indicates that the energy stability tends to be gentle. Obviously, declining trend and non-significant changes in C_v are beneficial for wind energy development.

Overall, C_v in most of the global oceans has no significant variation or significant declining trend in each season, indicating that wind energy stability tends to be better or stable, which is beneficial to wind energy development. Especially in the tropical Pacific Ocean, C_v shows a significant decreasing trend in all seasons.

In MAM (Fig. 8a), C_v in most global oceans has no significant variation or significantly decreasing trend. The regions with significant decreasing trend are mainly located in the equatorial waters of the South Pacific Ocean, the northeast trade wind area of the North Pacific, the marginal waters of the southeastern trade winds area of the South Pacific, the eastern part of Newfoundland, the western part of Liberia, the Somalian waters, the Sri Lankan waters, the equatorial South Indian Ocean, and the Arctic; that is, the stability of these areas tends to be better. The areas with significant increasing trend are mainly distributed in some scattered areas: the middle-low latitudes of the western Pacific, Anadyr Bay, and the northern edge of the Ross Sea, that is, the stability of these areas tended to be worse.

In JJA (Fig. 8b), C_v in most global oceans has no significant variation or significant decreasing trend. The regions with significant decreasing trend are mainly located in the central waters of the equatorial Pacific, the southeastern trade winds area of the South Pacific, and the eastern offshore region of South America. The areas with significant increasing trend are mainly distributed in the Arctic, the Gulf of Mexico, Icelandic waters, the northern edge of the Ross Sea, the Sea of Okhotsk, the Bering Sea, and some various other seas.

In SON (Fig. 8c), the low-latitude Pacific, the waters near Xindi Island, the Chukchi Sea, the Beaufort Sea, and the southern Icelandic waters have a significant decreasing trend. The areas with significant increasing trend are mainly distributed in the southeastern near-shore area of North America, the near-shore area of eastern Japan, and some other seas.

In DJF (Fig. 8d), the tropical South Pacific Ocean, the northeastern trade winds zone of the North Pacific, the equatorial South Atlantic, the Davis Strait, and the Southern Hemisphere westerly have a significant decreasing trend. Significantly increasing areas are mainly distributed in the Ross Sea, Hudson Bay, the Novosibirsk Islands to the Queen Elizabeth Islands, the Indonesian archipelago, and some sporadic waters.

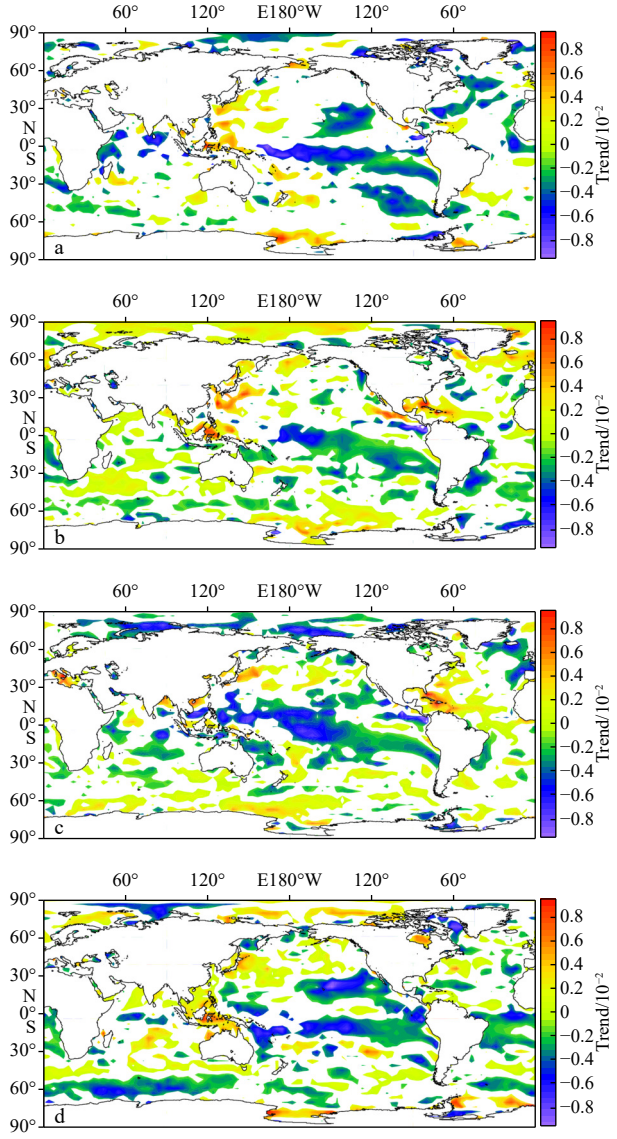

Fig. 8. Long-term trend of the coefficient of variation of wind power density in MAM (a), JJA (b), SON (c), and DJF (d) across the global ocean. Only areas significant at the 0.05 reliability level are colored.

4.2 *Monthly variability index*

Based on the year-by-year M_v data for the past 40 years obtained in Section 3.2, moving average method and linear regression are used to calculate the climatic variation of M_v, as shown in Fig. 9. A decrease in M_v indicates that the monthly variation tends to be smaller, while an increase in M_v indicates that the monthly variation tends to be larger. No significant change in M_v indicates a gentle trend in the monthly variation. It is not hard to understand that declining trend and non-significant changes in M_v are beneficial for wind energy development.

Obviously, most of the global oceans have significant decreases or non-significant variation in M_v. M_v decreases in the low latitudes of the Indian Ocean (–0.03 to –0.01 per year), the tropical Pacific Ocean (–0.03 to –0.01 per year), the middle and eastern mid-low latitudes of the Pacific Ocean (–0.005 to –0.015 per year), the Southern Hemisphere westerly (approximately –0.005 per year), and the Weddell Sea (–0.02 to –0.01 per year).

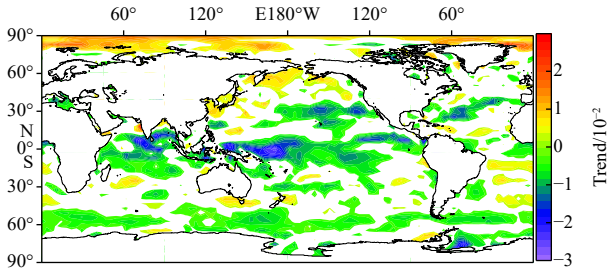

Fig. 9. Annual climatic trend of monthly variability index of wind power density in the global oceans. Only areas significant at the 0.05 reliability level are colored.

Significantly increasing areas are mainly distributed in the Arctic (0.01 to 0.02 per year), the waters around the Kamchatka Peninsula (0 to 0.02 per year), the Japan Sea (approximately 0.005 per year), and the East China Sea (approximately 0.01 per year). Overall, the areas with significantly increasing trends are mainly distributed in the high latitudes of the Northern Hemisphere. The areas with significantly decreasing trends are mainly distributed in low-latitude waters worldwide and the Southern Hemisphere.

4.3 *Seasonal variability index*

Based on the yearly S_v for the past 40 years obtained in Section 3.3, moving average and linear regression methods are used to calculate the climatic trend in S_v for 1979–2018, as shown in Fig. 10. A decrease in S_v indicates that the seasonal variation tends to be smaller. An increase in S_v indicates that the seasonal variation tends to be larger. Non-significant variation in S_v indicates a gentle trend in seasonal variation. Declining trend and non-significant changes in S_v are beneficial for wind energy development.

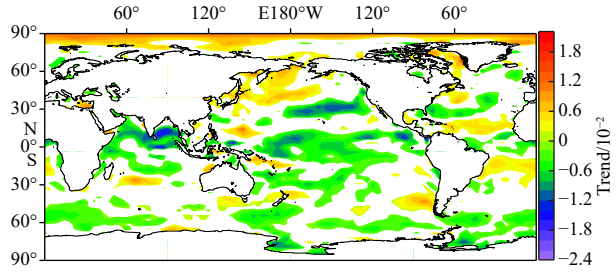

Fig. 10. Annual climatic trend of the seasonal variability index of wind power density in global oceans. Only areas significant at the 0.05 reliability level are colored.

The spatial distribution of the annual climatic trend in S_v (Fig. 10) maintain a good consistency with that in M_v (Fig. 9). The regions with significantly decreasing trends are located in the North Indian Ocean (–0.024 to –0.006 per year), the equatorial Pacific Ocean (approximately –0.006 per year), the 30°N waters of the North Pacific Ocean (–0.012 to –0.006 per year), the area southwest of New Zealand (approximately –0.004 per year), and the Weddell Sea (approximately –0.01 per year). Significantly increasing areas are mainly distributed in the central-western regions of the North Pacific westerly (0.002–0.008 per year), the Arctic region (0.006–0.012 per year), and the mid-low-latitude waters of the Atlantic Ocean (approximately 0.004 per year).

4.4 *Variation in stability in key regions*

This section emphasizes the low latitudes of the Pacific Ocean (30°S–30°N, 120°E–100°W) and the North Indian Ocean (0°–30°N, 30°–100°E), which exhibits obvious variations in C_v, M_v and S_v. The annual values of C_v, M_v and S_v of the WPD in the above two regions are presented in Fig. 11.

As shown in Fig. 11a, $|R| = \mathrm{SQRT}(R^2) = 0.14$, which did not pass the 0.1 level of significant reliability ($r_{0.1} = 0.26$). This result means that there is no significant variation in C_v of the North Indian Ocean for 1979–2018. Similarly, C_v in the low latitudes of the Pacific Ocean has no significant variation, as shown in Fig. 11b. However, C_v for the period 1997–2008 exhibits an obviously decreasing trend. As shown in Fig. 11c, $|R| = 0.23 < r_{0.1}$, which did not pass the 0.1 level of significant reliability. This result means

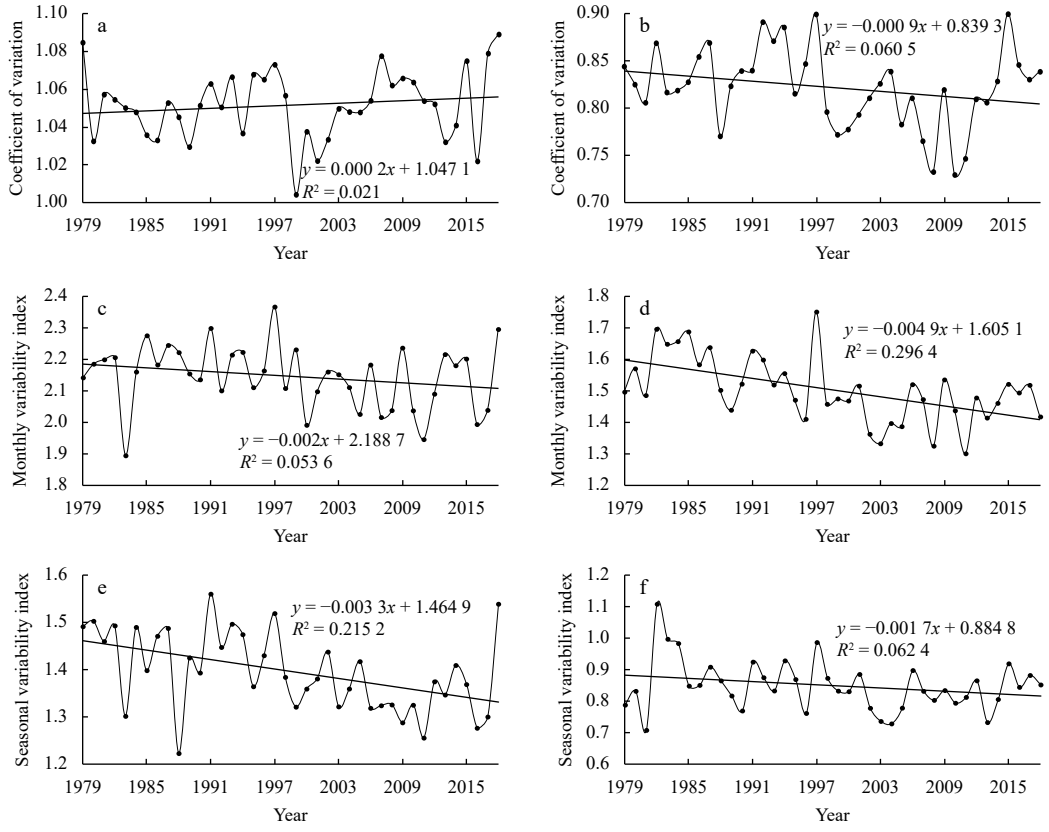

Fig. 11. Annual values of the coefficient of variation (a, b), monthly variability index (c, d), seasonal variability index (e, f) of wind power density in the North Indian Ocean (left) and low latitudes of the Pacific Ocean (right).

that M_v of the North Indian Ocean has no significant trend in the past 40 years. In Fig. 11d, $|R| = 0.54 > r_{0.001}$, and this value passed the 0.001 level of significant reliability. The regression coefficient is –0.004 9. This result means that M_v of the low latitudes of the Pacific Ocean exhibits a significantly decreasing trend of –0.004 9 per year over the past 40 years. A decreasing trend in M_v means that the monthly differences in resources tend to be narrow, which is beneficial for wind energy utilization. Similarly, S_v in the North Indian Ocean has an obvious decrease of –0.003 3 per year, while there is no significant variation of S_v in the low-latitude Pacific. The decreasing trend in S_v means that the seasonal differences in resources tend to be small, which is beneficial for wind energy utilization.

C_v in the North Indian Ocean exhibits a gentle variation in 1980–1998 and an increasing trend in 1999–2007. C_v in the low latitudes of the Pacific Ocean exhibits a gentle variation in 1979–1997, a decreasing trend in 1997–2008, and an increasing trend in 2010–2015. M_v in the North Indian Ocean exhibits a gentle variation over the past 40 years. M_v in the low latitudes of the Pacific Ocean exhibits a decreasing trend for two periods: 1982–1996 and 1997–2003. The decreasing trend of S_v is mainly dominated by the period of 1991–2011. In addition, S_v in 1997 exhibits a jump phenomenon. S_v in the low-latitude Pacific exhibits a gentle variation in 1985–2018.

The M-K test is used to analyze the abrupt phenomenon of C_v, M_v and S_v of the WPD in the low-latitude Pacific and North Indian Ocean, as shown in Fig. 12. In the results of the M-K test, there are four important lines, which are two test lines (dark black and light gray solid lines in Fig. 12a), and the UF and UB curves. When UF and UB intersect and the intersection point lies between the two test lines, it indicates the presence of a significant abrupt phenomenon. The abscissa corresponding to the intersection point is the abrupt time. In addition, the UF curve also shows the change trend of the analyzed elements.

As shown in Fig. 12a, the UF and UB lines intersect in 2007–2011. The intersection is located within two inspection lines. This result means that C_v of the North Indian Ocean has an obviously abrupt phenomenon for the period of 2007–2011. The UF line has no obvious variation, which verifies the accuracy of Fig. 11a.

In Fig. 12b, the UF and UB lines intersect in 1998, with the intersection located within the two inspection lines, meaning that C_v in the low-latitude Pacific has an obviously abrupt phenomenon in 1998. The UF line decreased obviously for the period of 1997–2008, which is in good agreement with Fig. 11b.

In Fig. 12c, M_v in the North Indian Ocean has an obvious abrupt phenomenon at the end of the 20th century (1998–2000). The UF line exhibits a significantly decreasing trend for the period of 2000–1012.

In Fig. 12d, M_v in the low latitudes of the Pacific Ocean has an obviously abrupt phenomenon in 1993. The UF line decreased obviously from 1985 to 2012, meaning this period has a significantly decreasing trend. The decreasing trend of M_v in the low latitudes of the Pacific Ocean is dominated by the period of

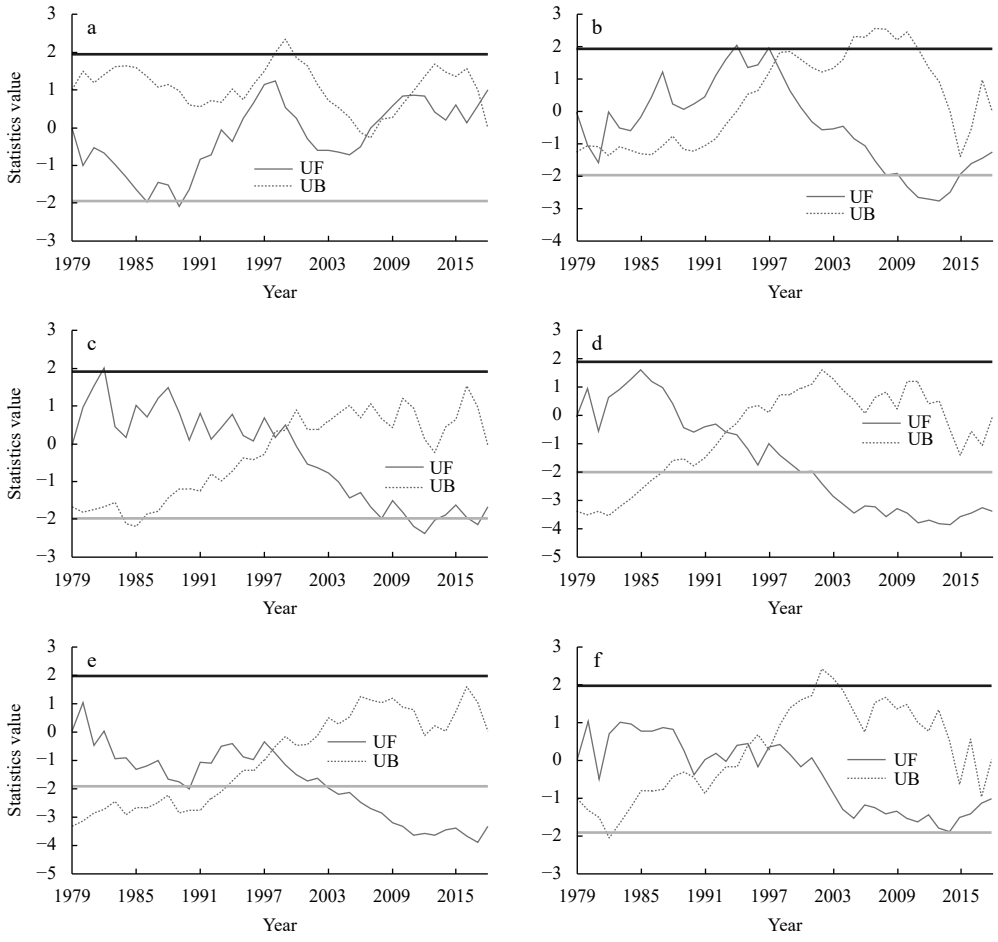

Fig. 12. M-K test of coefficient of variation (a, b), monthly variability index (c, d), seasonal variability index (e, f) of wind power density in the North Indian Ocean (left) and low latitudes of the Pacific Ocean (right). Dark black and light gray solid lines are two test lines.

1985–2012. This result verifies the accuracy of Fig. 11d.

In Fig. 12e, the UF and UB lines intersect in 1998. The intersection point is located within the two reliability test level lines. This result means that an obviously abrupt phenomenon of S_v occurred in 1998. From the UF line, S_v exhibits a significant decline for the period of 1997–2011, which is in good agreement with Fig. 11e.

In Fig. 12f, S_v in the low latitudes of the Pacific Ocean exhibits two abrupt points: 1995 and 1997. The UF line exhibits a gentle variation, which is in good agreement with Fig. 11f.

5 Conclusions and prospects

By using the ERA-Interim wind production data from the ECMWF, the spatial-temporal distribution, climatic trend and abrupt phenomenon of wind energy stability in the global oceans are calculated, systematically including three key stability indexes: C_v, M_v and S_v. The main conclusions are as follows.

(1) According to C_v, the wind energy stability in the trade wind zones and monsoon zones is better than that in the rest of the waters of the global oceans. The Southern Hemisphere westerly is better than that of the Northern Hemisphere. The North Pole is more stable than the South Pole. Greenland and the South Pole have the worst stability worldwide. There are 6 regions with good perennial stability in the world (the northeast trade wind area of the North Pacific, the southeast trade wind area of the South Pacific, the northeast trade wind area of the Atlantic, the southeast trade wind area of the South Atlantic, the southeast trade wind area of the South Indian Ocean, and the Southern Hemisphere westerly waters, with C_v values below 0.8 all year round), and there is a semi-permanently stable zone (monsoon area in the North Indian Ocean).

(2) The best season for the stability of wind energy varies from sea to sea. The stability of the westerly zones in the Southern and Northern Hemispheres is best in winter and worst in summer. The stability in the North Indian Ocean and southeast trade zones of the South Indian Ocean is best in JJA. The southeast trade wind areas of the Atlantic and Pacific are best in SON. The northeast trade wind areas of the Atlantic and Pacific are best in MAM.

(3) There are six low-value areas of M_v: the northeast trade wind area of the North Pacific, the southeast trade wind area of the South Pacific, the northeast trade wind area of the Atlantic, the southeast trade wind area of the South Atlantic, the southeast trade wind area of South Indian Ocean, and the Southern Hemisphere westerly waters, with M_v values below 1.0. The Southern Hemisphere has an overall smaller monthly variation than that in the Northern Hemisphere. The M_v in the Arabian Sea is the largest worldwide, with a value even greater than 3.0. Overall, the spatial distribution characteristic of S_v maintains a good consistency with that of M_v. But the value of S_v is slightly lower than that of M_v.

(4) For the past 40 years, most of the global oceans experienced a significant decrease or non-significant variation in C_v. Only some sporadic sea areas had a significant increase in C_v. This pattern is beneficial for wind energy development. Areas with a significant decrease in C_v are mainly located in the southeast trade wind area of the South Pacific, northeast trade wind area of the North Pacific and equatorial Pacific, with significantly decreasing trends in all seasons.

(5) Most global oceans have a significant decrease or non-significant variation in M_v. The regions with significant decreases are located in the Indian Ocean-Pacific low latitudes (–0.03 to –0.01 per year) and the Southern Hemisphere westerly (approximately –0.005 per year). Significantly increasing areas are mainly distributed in the Arctic (0.01–0.02 per year), the waters around the Kamchatka Peninsula (0–0.02 per year), the Japan Sea (approximately 0.005 per year), and the East China Sea (approximately 0.01 per year). The spatial distribution characteristic of the annual climatic trend in S_v maintains a good consistency with that in M_v. That is, the monthly and seasonal variability tend to be shrink/smooth, which is beneficial for wind energy utilization.

(6) C_v in the North Indian Ocean did not exhibit an obviously abrupt phenomenon. The abrupt phenomenon of C_v in the low-latitude Pacific occurred in 1998. M_v and S_v of the North Indian Ocean and the low-latitude Pacific have obviously abrupt phenomenon that occurred at the end of the 20th century. The decreasing trend of M_v in the low latitudes of the Pacific Ocean was dominated by the period of 1985–2012. The significantly decline trend of S_v in the low-latitude Pacific Ocean was mainly dominated by 1997–2011.

In this study, the ERA-Interim production is used to analyze the climatic variation in global oceanic wind energy stability. Recently, the ERA5 reanalysis is made available, which shows a 20% improvement relative to ERA-Interim (Rivas and Stoffelen, 2019). In future work, the ERA5 production can also be used in wind energy assessments.

In 2019, deCastro et al. (2019) presented an overview of offshore wind energy resources in Europe under present and future climate. They pointed out that the regions have no variation or increase in wind energy in the future appearing to be suitable for installing or maintaining offshore wind farms. This work provided a key guidance for the long-term planning of wind energy development. In 2021, Carvalho et al. (2021) took advance in carrying out a long-term projection of wind energy in the Europe by using CMIP6 data. They pointed out that the future trend varied under condition of SSP2-4.5 and SSP5-8.5. This study mainly presented the climatic trend of stability of wind energy. Referring to deCastro et al. (2019) and Carvalho et al. (2021), it is also necessary to carry out the future projection of the stability of wind energy, to provide a scientific reference for the future utilization plan of wind energy. Research shows that there is a close relationship between wind energy resource and North Atlantic Oscillation (NAO) in the North Atlantic Ocean (Zheng et al., 2017). In the future work, it is also necessary to carry out the analysis of the relationship between the stability of wind energy and important climate systems, such as Pacific Decadal Oscillation (PDO), El Niño-Southern Oscillation (ENSO), Indian Ocean Dipole (IOD) and so on, thus to detect the inherent physical mechanism of change trend of wind energy stability.

Acknowledgements

The author would like to thank the ECMWF for providing the ERA-Interim wind data (available at https://apps.ecmwf.int/datasets/data/Interim-full-daily/levtype=sfc/).

References

Allen D J, Tomlin A S, Bale C S E, et al. 2017. A boundary layer scaling technique for estimating near-surface wind energy using numerical weather prediction and wind map data. Applied Energy, 208: 1246–1257, doi: 10.1016/j.apenergy.2017.09.029

Allouhi A, Zamzoum O, Islam M R, et al. 2017. Evaluation of wind energy potential in Morocco's coastal regions. Renewable and Sustainable Energy Reviews, 72: 311–324, doi: 10.1016/j.rser.2017.01.047

Capps S B, Zender C S. 2010. Estimated global ocean wind power potential from QuikSCAT observations, accounting for turbine characteristics and siting. Journal of Geophysical Research: Atmospheres, 115(D9): D09101, doi: 10.1029/2009JD012679

Carvalho D, Rocha A, Gómez-Gesteira M, et al. 2014. WRF wind sim-

ulation and wind energy production estimates forced by different reanalyses: Comparison with observed data for Portugal. Applied Energy, 117: 116–126, doi: 10.1016/j.apenergy.2013.12.001

Carvalho D, Rocha A, Gómez-Gesteira M, et al. 2017a. Offshore winds and wind energy production estimates derived from ASCAT, OSCAT, numerical weather prediction models and buoys—A comparative study for the Iberian Peninsula Atlantic coast. Renewable Energy, 102: 433–444, doi: 10.1016/j.renene.2016.10.063

Carvalho D, Rocha A, Gómez-Gesteira M, et al. 2017b. Potential impacts of climate change on European wind energy resource under the CMIP5 future climate projections. Renewable Energy, 101: 29–40, doi: 10.1016/j.renene.2016.08.036

Carvalho D, Rocha A, Costoya X, et al. 2021. Wind energy resource over Europe under CMIP6 future climate projections: What changes from CMIP5 to CMIP6. Renewable and Sustainable Energy Reviews, 151: 111594, doi: 10.1016/j.rser.2021.111594

Chadee X T, Clarke R M. 2014. Large-scale wind energy potential of the Caribbean region using near-surface reanalysis data. Renewable and Sustainable Energy Reviews, 30: 45–58, doi: 10.1016/j.rser.2013.09.018

Cornett A M. 2008. A global wave energy resource assessment. In: Proceedings of the 18th International Offshore and Polar Engineering Conference. Vancouver, Canada: International Society of Offshore and Polar Engineers, 318–326

Costoya X, deCastro M, Carvalho D, et al. 2021. Climate change impacts on the future offshore wind energy resource in China. Renewable Energy, 175: 731–747, doi: 10.1016/j.renene.2021.05.001

Davy R, Gnatiuk N, Pettersson L, et al. 2018. Climate change impacts on wind energy potential in the European domain with a focus on the Black Sea. Renewable and Sustainable Energy Reviews, 81: 1652–1659, doi: 10.1016/j.rser.2017.05.253

deCastro M, Costoya X, Salvador S, et al. 2019. An overview of offshore wind energy resources in Europe under present and future climate. Annals of the New York Academy of Sciences, 1436(1): 70–97, doi: 10.1111/nyas.13924

Dee D P, Uppala S M, Simmons A J, et al. 2011. The ERA-Interim reanalysis: configuration and performance of the data assimilation system. Quarterly Journal of the Royal Meteorological Society, 137(656): 553–597, doi: 10.1002/qj.828

Esteban M D, Espada J M, Ortega J M, et al. 2019. What about marine renewable energies in Spain?. Journal of Marine Science and Engineering, 7(8): 249, doi: 10.3390/jmse7080249

González-Longatt F, González J S, Payán M B, et al. 2014. Wind-resource atlas of Venezuela based on on-site anemometry observation. Renewable and Sustainable Energy Reviews, 39: 898–911, doi: 10.1016/j.rser.2014.07.172

Han Li, Romero C E, Yao Zheng. 2015. Wind power forecasting based on principle component phase space reconstruction. Renewable Energy, 81: 737–744, doi: 10.1016/j.renene.2015.03.037

Jung C, Taubert D, Schindler D. 2019. The temporal variability of global wind energy—Long-term trends and inter-annual variability. Energy Conversion and Management, 188: 462–472, doi: 10.1016/j.enconman.2019.03.072

Kumar B P, Vialard J, Lengaigne M, et al. 2013. TropFlux wind stresses over the tropical oceans: evaluation and comparison with other products. Climate Dynamics, 40(7): 2049–2071

Langodan S, Cavaleri L, Viswanadhapalli Y, et al. 2014. The Red Sea: a natural laboratory for wind and wave modeling. Journal of Physical Oceanography, 44(12): 3139–3159, doi: 10.1175/JPO-D-13-0242.1

Langodan S, Viswanadhapalli Y, Dasari H P, et al. 2016. A high-resolution assessment of wind and wave energy potentials in the Red Sea. Applied Energy, 181: 244–255, doi: 10.1016/j.apenergy.2016.08.076

Liu Hui, Chen Chao. 2019. Data processing strategies in wind energy forecasting models and applications: A comprehensive review. Applied Energy, 249: 392–408, doi: 10.1016/j.apenergy.2019.04.188

Liu Fa, Sun Fubao, Liu Wenbin, et al. 2019. On wind speed pattern and energy potential in China. Applied Energy, 236: 867–876, doi: 10.1016/j.apenergy.2018.12.056

Marcos R, González-Reviriego N, Torralba V, et al. 2019. Characterization of the near surface wind speed distribution at global scale: ERA-Interim reanalysis and ECMWF seasonal forecasting system 4. Climate Dynamics, 52(5/6): 3307–3319, doi: 10.1007/s00382-018-4338-5

Omrani H, Drobinski P, Arsouze T, et al. 2017. Spatial and temporal variability of wind energy resource and production over the North Western Mediterranean Sea: Sensitivity to air-sea interactions. Renewable Energy, 101: 680–689, doi: 10.1016/j.renene.2016.09.028

Onea F, Deleanu L, Rusu L, et al. 2016. Evaluation of the wind energy potential along the Mediterranean Sea coasts. Energy Exploration & Exploitation, 34(5): 766–792

Pryor S C, Barthelmie R J. 2011. Assessing climate change impacts on the near-term stability of the wind energy resource over the United States. Proceedings of the National Academy of Sciences of the United States of America, 108(20): 8167–8171, doi: 10.1073/pnas.1019388108

Qian Zheng, Pei Yan, Zareipour H, et al. 2019. A review and discussion of decomposition-based hybrid models for wind energy forecasting applications. Applied Energy, 235: 939–953, doi: 10.1016/j.apenergy.2018.10.080

Rivas M B, Stoffelen A. 2019. Characterizing ERA-Interim and ERA5 surface wind biases using ASCAT. Ocean Science, 15(3): 831–852, doi: 10.5194/os-15-831-2019

Rusu L, Ganea D, Mereuta E. 2018. A joint evaluation of wave and wind energy resources in the Black Sea based on 20-year hindcast information. Energy Exploration & Exploitation, 36(2): 335–351

Rusu L, Onea F. 2017. The performance of some state-of-the-art wave energy converters in locations with the worldwide highest wave power. Renewable and Sustainable Energy Reviews, 75: 1348–1362, doi: 10.1016/j.rser.2016.11.123

Song Lina, Liu Zhiliang, Wang Fan. 2015. Comparison of wind data from ERA-Interim and buoys in the Yellow and East China Seas. Chinese Journal of Oceanology and Limnology, 33(1): 282–288, doi: 10.1007/s00343-015-3326-4

Soukissian T H, Denaxa D, Karathanasi F, et al. 2017. Marine renewable energy in the Mediterranean Sea: Status and perspectives. Energies, 10(10): 1512, doi: 10.3390/en10101512

Soukissian T H, Karathanasi F E. 2016. On the use of robust regression methods in wind speed assessment. Renewable Energy, 99: 1287–1298, doi: 10.1016/j.renene.2016.08.009

Thomas B R, Kent E C, Swail V R, et al. 2008. Trends in ship wind speeds adjusted for observation method and height. International Journal of Climatology, 28(6): 747–763, doi: 10.1002/joc.1570

Ulazia A, Sáenz J, Ibarra-Berastegui G, et al. 2017. Using 3DVAR data assimilation to measure offshore wind energy potential at different turbine heights in the West Mediterranean. Applied Energy, 208: 1232–1245, doi: 10.1016/j.apenergy.2017.09.030

Wan Yong, Fan Chenqing, Dai Yongshou, et al. 2018. Assessment of the joint development potential of wave and wind energy in the South China Sea. Energies, 11(2): 398, doi: 10.3390/en11020398

Wan Yong, Zhang Jie, Meng Junmin, et al. 2015. Exploitable wave energy assessment based on ERA-Interim reanalysis data—A case study in the East China Sea and the South China Sea. Acta Oceanologica Sinica, 34(9): 143–155, doi: 10.1007/s13131-015-0641-8

Wang Yihui, Walter R K, White C, et al. 2019. Assessment of surface wind datasets for estimating offshore wind energy along the Central California Coast. Renewable Energy, 133: 343–353, doi: 10.1016/j.renene.2018.10.008

Wang Guosong, Wang Xidong, Wang Hui, et al. 2020. Evaluation on monthly sea surface wind speed of four reanalysis data sets over the China seas after 1988. Acta Oceanologica Sinica, 39(1): 83–90, doi: 10.1007/s13131-019-1525-0

Xydis G. 2015. A wind energy integration analysis using wind re-

source assessment as a decision tool for promoting sustainable energy utilization in agriculture. Journal of Cleaner Production, 96: 476–485, doi: 10.1016/j.jclepro.2013.11.030

Xydis G, Mihet-Popa L. 2017. Wind energy integration via residential appliances. Energy Efficiency, 10(2): 319–329, doi: 10.1007/s12053-016-9459-2

Yan Jie, Zhang Hao, Liu Yongqian, et al. 2019. Uncertainty estimation for wind energy conversion by probabilistic wind turbine power curve modelling. Applied Energy, 239: 1356–1370, doi: 10.1016/j.apenergy.2019.01.180

Yu Lejiang, Zhong Shiyuan. 2019. The Interannual variability of surface winds in Antarctica and the surrounding oceans: A climatological analysis using the ERA-Interim reanalysis data. Journal of Geophysical Research: Atmospheres, 124(16): 9046–9061, doi: 10.1029/2019JD030328

Zheng Chongwei, Li Chongyin, Li Xin. 2017. Recent decadal trend in the North Atlantic wind energy resources. Advances in Meteorology, 2017: 7257492, doi: 10.1155/2017/7257492

Zheng Chongwei, Li Xueyan, Luo Xia, et al. 2019a. Projection of future global offshore wind energy resources using CMIP data. Atmosphere: Ocean, 57(2): 134–148, doi: 10.1080/07055900.2019.1624497

Zheng Chongwei, Li Chongyin, Xu Jianjun. 2019b. Micro-scale classification of offshore wind energy resource—A case study of the New Zealand. Journal of Cleaner Production, 226: 133–141, doi: 10.1016/j.jclepro.2019.04.082

Zheng Chongwei, Xiao Ziniu, Peng Yuehua, et al. 2018. Rezoning global offshore wind energy resources. Renewable Energy, 129: 1–11, doi: 10.1016/j.renene.2018.05.090